Lattice QCD Phase Diagram In and Away from the Strong Coupling Limit

Ph. de Forcrand,[1,2] J. Langelage,[1] O. Philipsen,[3] and W. Unger[3]
[1]Institut für Theoretische Physik, ETH Zürich, CH-8093 Zürich, Switzerland
[2]CERN, Physics Department, TH Unit, CH-1211 Geneva 23, Switzerland
[3]Institut für Theoretische Physik, Goethe-Universität Frankfurt, 60438 Frankfurt am Main, Germany
(Received 17 June 2014; published 6 October 2014)

We study lattice QCD with four flavors of staggered quarks. In the limit of infinite gauge coupling, "dual" variables can be introduced, which render the finite-density sign problem mild and allow a full determination of the $\mu - T$ phase diagram by Monte Carlo simulations, also in the chiral limit. However, the continuum limit coincides with the weak coupling limit. We propose a strong-coupling expansion approach towards the continuum limit. We show first results, including the phase diagram and its chiral critical point, from this expansion truncated at next-to-leading order.

DOI: 10.1103/PhysRevLett.113.152002 PACS numbers: 12.38.Gc, 12.38.Aw, 21.65.-f

The properties of QCD as a function of temperature T and matter density are summarized by its phase diagram, whose determination is a major goal of heavy-ion experiments. Although the quark-gluon plasma has been observed at high temperature, further features of the phase diagram, especially a possible QCD critical point, have not been identified yet. Heroic efforts have been devoted to numerical lattice simulations, which are the appropriate tool for nonperturbative phenomena like phase transitions. However, the fermion determinant becomes complex upon turning on a chemical potential μ coupled to the quark number. This so-called "sign problem" requires prohibitively large computer resources growing exponentially with the lattice 4-volume. Approaches to circumvent this problem are applicable when $\mu/T \lesssim 1$ only [1], and results on the QCD critical point are inconclusive. We want to make progress on this problem by means of a strong coupling expansion as applied to zero density in the early days of lattice gauge theory or, recently, to finite temperature and density with heavy quarks [2,3]. Here we want to address the opposite, chiral limit with a different strategy [4,5]. Note that both for heavy and chiral quarks, the strong coupling approach gives access also to the cold and dense regime of nuclear matter [3,6,7].

The sign problem occurs when elements $\langle\psi_i|\exp(-\delta\tau H)|\psi_j\rangle$ of the transfer matrix between states $|\psi_i\rangle$ and $|\psi_j\rangle$ sampled by Monte Carlo simulations become negative. This problem is representation dependent: in an eigenbasis of the Hamiltonian, all matrix elements would be non-negative. Thus, the sign problem will become milder if we can express the partition function in terms of approximate eigenstates. We know that QCD eigenstates are color singlets. Therefore, instead of performing Monte Carlo calculations on colored gauge links, as in the usual approach, we integrate the gauge links *first*, and work with the resulting color singlets. This strategy becomes particularly practical in the strong coupling limit. Here, we reexpress the partition function as a sum over configurations of hadron worldlines, similar to the "dual variables" used in [8]. The resulting sign problem is extremely mild, allowing us to simulate large lattices at arbitrarily large chemical potentials, and reliably obtain the full phase diagram. Of course, in the strong coupling limit $g \to \infty, \beta = 2N_c/g^2 \to 0$ (for N_c colors), the lattice is maximally coarse, whereas the continuum limit coincides with the weak coupling limit $g \to 0, \beta \to \infty$. In this Letter, we first summarize the $\beta = 0$ phase diagram and then explain how to include the first $\mathcal{O}(\beta)$ corrections, which allows us to measure Wilson loops at $\beta = 0$ and fermionic observables at $\mathcal{O}(\beta)$. We then present the QCD phase diagram for small $\beta > 0$. For $\mu = 0$, where we can cross-check with the full Monte Carlo approach, perfect agreement is found for small β.

We adopt the staggered fermion discretization and the Wilson plaquette action with the partition function

$$Z_{\mathrm{QCD}} = \int d\psi d\bar{\psi} dU e^{S_G + S_F},$$
$$S_G = \frac{\beta}{2N_c}\sum_P \mathrm{tr}[U_P + U_P^\dagger], \tag{1}$$

$$S_F = am_q \sum_x \bar{\psi}_x \psi_x + \frac{1}{2}\sum_{x,\nu} \eta_\nu(x)\gamma^{\delta_{\nu 0}} \times [\bar{\psi}_x e^{a_t\mu\delta_{\nu 0}} U_\nu(x)\psi_{x+\hat{\nu}} - \bar{\psi}_{x+\hat{\nu}} e^{-a_t\mu\delta_{\nu 0}} U_\nu^\dagger(x)\psi_x], \tag{2}$$

with a and a_t the spatial and temporal lattice spacings, γ the anisotropy by which one may tune a/a_t, m_q the quark mass, and μ the quark chemical potential. The η's are the usual ± 1 staggered phases. In the continuum limit $g \to 0$, our action describes QCD with 4 mass-degenerate quark species. In the opposite limit $g \to \infty$, the plaquette, four-link coupling β vanishes and so does the gauge action S_G. Then, the integration over the links $U_\nu(x)$ factorizes into a

product of one-link integrals which can be carried out analytically [9]. Finally, one performs the Grassmann integration over the fermion fields $\psi(x), \bar{\psi}(x)$, and obtains the partition function in terms of color-singlet degrees of freedom (mesons and baryons) [4], as a sum over discrete graphs on the lattice (with $N_c = 3$ for QCD):

$$Z_{SC} = \sum_{\{n,k,\ell\}} \prod_x w_x \prod_b w_b \prod_\ell w_\ell \tag{3}$$

$$w_x = \frac{N_c!}{n_x!}(2am_q)^{n_x}; \qquad w_b = \frac{(N_c - k_b)!}{N_c! k_b!}. \tag{4}$$

The mesons are represented by monomers $n_x \in \{0, \ldots, N_c\}$ on sites x and dimers $k_b \in \{0, \ldots, N_c\}$ on bonds $b = (x, \hat{\nu})$, whereas the baryons are represented by oriented self-avoiding loops ℓ. The weight w_ℓ of a baryonic loop ℓ and its sign depend on the loop geometry [10]. Configurations $\{n, k, \ell\}$ must satisfy at each site x the constraint inherited from Grassmann integration:

$$n_x + \sum_{\hat{\nu}=\pm\hat{0},\ldots,\pm\hat{d}} \left(k_{\hat{\nu}}(x) + \frac{N_c}{2} |\ell_{\hat{\nu}}(x)| \right) = N_c, \tag{5}$$

which implies that mesonic degrees of freedom cannot occupy baryonic sites.

This system has been studied for decades, both via mean field [11–16] and by Monte Carlo methods [5,7,10]. In recent years, the latter have undergone a revival using the worm algorithm [7,17,18], which violates the Grassmann constraint in order to sample the monomer two-point function $G(x, y)$, from which the chiral susceptibility can be obtained. These techniques have been applied to obtain all lattice data presented here. We study the chiral limit $m_q = 0$, which does not incur a penalty in computer cost, contrary to the usual determinantal approach. The staggered action S_F Eq. (2) then satisfies a $U(1)$ "remnant" chiral symmetry, which is spontaneously broken at low temperature and density, with order parameter $\langle\bar{\psi}\psi\rangle$. In Fig. 1 left, we show the (μ, T) phase diagram in the strong-coupling limit. It is qualitatively similar to the expected phase diagram of QCD in the chiral limit: the transition is of second order from $a\mu = 0$ up to a tricritical point $(a\mu_T, aT_T)$, then turns first order. At finite quark mass, the second order line turns into a crossover and the tricritical point into a second order critical endpoint. Note the different phase boundaries obtained from lattices with different numbers N_t of time slices: they converge to the continuous-time phase boundary as $N_t \to \infty$. The $1/N_t$ corrections can be absorbed in a parametrization of $a/a_t = f(\gamma)$, with γ the anisotropy needed to reach temperatures $aT > 1/2$ [18], resulting in Fig. 1, right [19].

A crucial question is whether this phase diagram develops new features as β is increased from 0 to ∞. At low temperature especially, things may change: when $\beta = 0$,

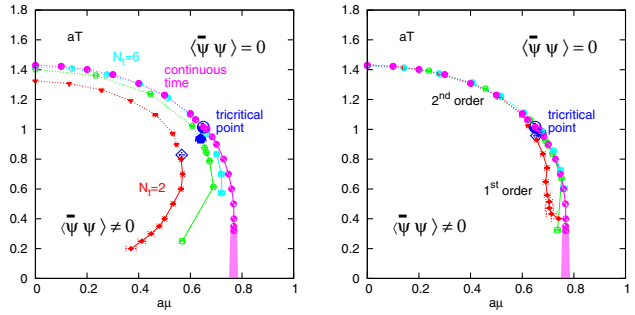

FIG. 1 (color online). Left: Lattice QCD phase diagram in the strong coupling limit, setting $a/a_t = \gamma^2$ following mean field. Different results are obtained for different numbers N_t of time slices $N_t = 2$, $N_t = 4$ [7], $N_t = 6$, and $N_t = \infty$ (i.e., continuous Euclidean time) [18]. Right: Same, with corrected anisotropy [19].

the transition at $\mu_c(T = 0)$ separates a chirally broken, baryon-free vacuum and a chirally symmetric, baryon-saturated state with one static baryon per lattice site. That is a very crude cartoon of a nuclear matter phase: in the continuum limit, depending on μ, it may evolve into a nuclear liquid, a crystalline phase, a color superconductor, etc. A first insight may be gained by considering $\mathcal{O}(\beta)$ corrections to the $\beta = 0$ phase diagram. At the same time, we can also address an interesting quantitative issue: the ratio $T_c(\mu = 0)/\mu_c(T = 0)$ is about $(160\,\mathrm{MeV})/(300\,\mathrm{MeV})$ ~ 0.53 in nature, but about $1.402/0.75 \approx 1.87$ when $\beta = 0$. How does it vary with β?

Corrections to the strong coupling limit.—To go beyond the strong coupling limit, a systematic expansion in β of the partition function is needed, which we perform to first order. Writing the $\beta = 0$ partition function as $Z_{SC} = \int d\psi d\bar{\psi} Z_F$, with $Z_F(\psi, \bar{\psi}) = \int dU e^{S_F}$ the fermionic partition function, the $\beta \neq 0$ partition function Eq. (1) becomes

$$Z_{\mathrm{QCD}} = \int d\psi d\bar{\psi} dU e^{S_F + S_G} = \int d\psi d\bar{\psi} Z_F \langle e^{S_G} \rangle_{Z_F}, \tag{6}$$

$$\langle e^{S_G} \rangle_{Z_F} \simeq 1 + \langle S_G \rangle_{Z_F} = 1 + \frac{\beta}{2N_c} \sum_P \langle \mathrm{tr}[U_P + U_P^\dagger] \rangle_{Z_F}, \tag{7}$$

where Eq. (7) is an $\mathcal{O}(\beta)$ truncation. We thus need the expectation value of the elementary plaquette $\mathrm{tr}[U_P]$ in the strong coupling ensemble Z_F. The plaquette is composed of 4 links representing gluons, which provide new possibilities to make color singlets together with $\bar{\psi}_x \psi_{x\pm\hat{\mu}}$ propagating fermions. The modifications to the partition function are computed from the product $U_P = J_{ij} J_{jk} J_{kl} J_{li}$ of the one-link integrals $J_{ij} \equiv \int dU U_{ij} \exp(\bar{\psi} U \phi - \bar{\phi} U^\dagger \psi)$ around an elementary plaquette [20–22]

$$J_{ij} = -\sum_{k=1}^{3} \frac{(3-k)!}{3!(k-1)!} [M_\psi M_\phi]^{k-1} \bar{\phi}_j \psi_i + \frac{1}{12} \varepsilon_{ii_2i_3} \varepsilon_{jj_2j_3} \bar{\psi}_{i_2} \phi_{j_2} \bar{\psi}_{i_3} \phi_{j_3} - \frac{1}{3} \bar{B}_\psi B_\phi \bar{\phi}_j \psi_i, \quad (8)$$

where M and B represent mesons and baryons. The first term describes the propagation of a $(\bar{q}g)$ antiquark plus gluon together with 0 to 2 mesons, the second term describes a (qqg), the third term is a $(\bar{q}g)$ together with a baryon. From these, we compute the weight associated with a plaquette source term in the strong coupling configuration.

At the corners of the plaquette, the Grassmann variables ψ, ϕ are bound into baryons and mesons. Introducing a variable $q_P \in \{0, 1\}$ to mark the "excited" plaquettes P associated with the second term of Eq. (7), and corresponding variables q_b and $q_x = q_P$ for the links and the corners of such plaquettes, we can write the $\mathcal{O}(\beta)$ partition function in the same form as Eq. (3) with modified weights $\hat{w}$:

$$Z(\beta) = \sum_{\{n,k,\ell,q_P\}} \prod_x \hat{w}_x \prod_b \hat{w}_b \prod_\ell \hat{w}_\ell \prod_P \hat{w}_P \quad (9)$$

$$\hat{w}_x = w_x v_x, \qquad \hat{w}_b = w_b k_b^{q_b}, \quad (10)$$

$$\hat{w}_\ell = w_\ell \prod_\ell w_{B_i}(\ell), \qquad \hat{w}_P = \left(\frac{\beta}{2N_c}\right)^{q_P}, \quad (11)$$

where $v_x = (N_c - 1)!$ if x is the corner of an excited plaquette attached to an external meson line, $N_c!$ if it is attached to an external baryon line, 1 otherwise. Likewise, the weight of each baryon loop segment l is modified by a factor $w_{B_1} = 1/(N_c - 1)!$, $w_{B_2} = (N_c - 1)!$, where B_1 and B_2 correspond to the second and third expression in Eq. (8). We can sample this partition function by the same worm algorithm as for $\beta = 0$, adding a Metropolis step to update the plaquette variables q_P. In practice, we found it simpler to reweight from the $\beta = 0$ ensemble.

Qualitatively new features from $\mathcal{O}(\beta)$ contributions are as follows: (i) The constituent quarks of baryons and mesons can now separate; hadrons are no longer pointlike, but acquire a size $\sim a$. (ii) The baryon-baryon interaction can now proceed by quark exchange: it is no longer limited to the on-site Pauli exclusion principle. (iii) Chiral symmetry breaking becomes possible even in the dense phase similar to nuclear matter.

Wilson loops at $\beta = 0$.—Figure 2 illustrates the dependence of the Polyakov loop and of the plaquette (timelike and spacelike) on the chemical potential μ and the temperature T, at $\beta = 0$. The x axis represents the "distance" $a\sqrt{\mu^2 + T^2}$ from the vacuum, and different symbols are used for different values of μ/T. Several features are noticeable. (i) The plaquette has a nonzero value caused by the ordering effect of the fermions. Indeed, increasing

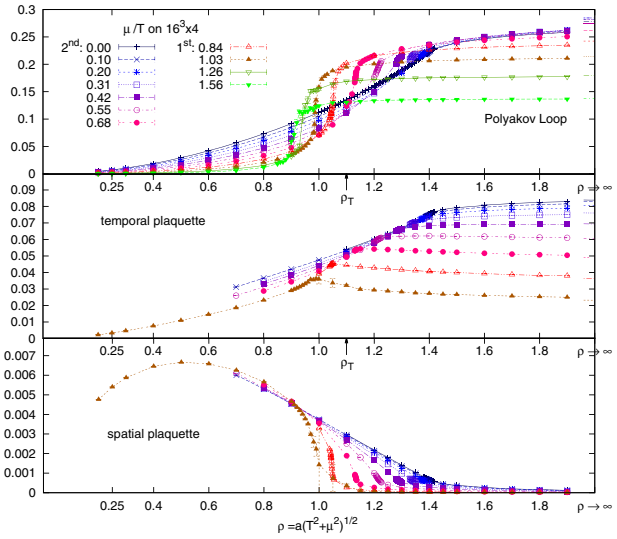

FIG. 2 (color online). Polyakov loop $\frac{1}{3}\langle \mathrm{tr} L \rangle$ and average spatial and temporal plaquette $\frac{1}{3}\langle \mathrm{tr} P_s \rangle$, $\frac{1}{3}\langle \mathrm{tr} P_t \rangle$ as a function of (μ, T) on a $16^3 \times 4$ lattice at $\beta = 0$. The colors label successive values of μ/T, and the x axis is $\rho \equiv a\sqrt{\mu^2 + T^2}$. At the tricritical point, $\rho_T = 1.10(2)$. Wilson loops are sensitive to the chiral transition and develop a discontinuity as the transition turns first order. $\langle \mathrm{tr} P_s \rangle$ varies oppositely to $\langle \mathrm{tr} P_t \rangle$, and remains very small.

the number of quark fields from 1 to 13 triggers restoration of the chiral symmetry [23]. (ii) The first-order phase transition is visible at large μ/T through a discontinuity in all Wilson loops, although it is associated with chiral symmetry. This can be assigned to the nonzero latent heat. (iii) Even in the regime of small μ/T, where the chiral transition is second order, the Polyakov loop is clearly sensitive to the transition as already found in U(3) gauge theory [24], reflecting the "entanglement" of confinement and chiral symmetry seen in effective models [25].

Phase diagram as a function of β.—We now show how to obtain the derivative $d(aT_c)/d\beta|_{\beta=0}$ of the chiral transition temperature aT_c with respect to β. Since the worm algorithm samples the two-point correlation function $G(x_1, x_2)$, we can measure its integral, which is equal to the chiral susceptibility χ (there is no disconnected piece $\langle \bar{\psi}\psi \rangle^2$ at $m_q = 0$ and in a finite volume, since $\langle \bar{\psi}\psi \rangle = 0$ also in the chirally broken phase),

$$\chi \equiv \langle (\bar{\psi}\psi)^2 \rangle = \frac{1}{L^3 N_t} \sum_{x_1, x_2} G(x_1, x_2). \quad (12)$$

At $\beta = 0$ and for some $\mu < \mu_T$, the critical temperature $aT_c(\mu)$ can be obtained from finite-size scaling: the curves $\chi(aT, L)L^{-\gamma/\nu}$ obtained on several lattice sizes L all intersect at $T = T_c(\mu)$, with a slope $\propto L^{1/\nu}$ at the intersection, as illustrated Fig. 3, left. The transition is in the $3dO(2)$ universality class with known critical exponents, which facilitates the analysis. In the region of a first-order

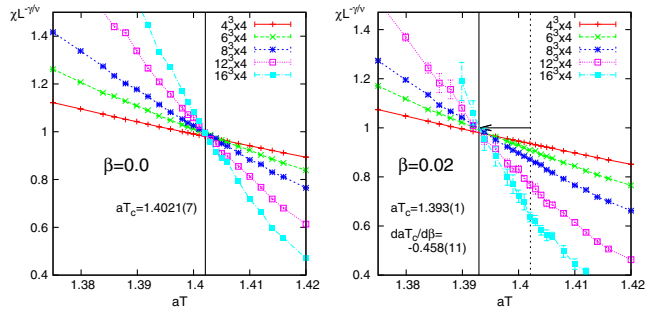

FIG. 3 (color online). The $\mu = 0$ transition temperature aT_c from finite-size scaling of the chiral susceptibility on $N_t = 4$ lattices. Left: $\beta = 0$. Right: $\beta = 0.02$. The arrow marks the shift in aT_c.

transition, $\mu > \mu_T$, this ansatz is modified following Ref. [26]. When we turn on β, the chiral susceptibility changes and we can measure its derivative

$$\frac{d\chi}{d\beta} = 3L^3 N_t(\langle\langle(\bar{\psi}\psi)^2 P_t\rangle - \langle(\bar{\psi}\psi)^2\rangle\langle P_t\rangle\rangle). \tag{13}$$

While both the temporal and the spatial plaquettes formally enter in this expression, the latter is a factor $\gtrsim 10$ smaller than the former; cf. Fig. 2. The effect of β, to linear order, is illustrated in Fig. 3, right. At temperature aT_c, the rescaled chiral susceptibility $\chi L^{-\gamma/\nu}$ changes by $\beta(d\chi/d\beta)L^{-\gamma/\nu}$ [19], which produces a horizontal shift of the intersection point. At $\mu = 0$ (on $N_t = 4$ lattices), $aT_c|_{\beta=0} = 1.4021(7)$, $(d/d\beta)aT_c(\beta)|_{\beta=0} = -0.46(1)$.

We find that aT_c decreases as β increases: this is expected since a decreases. Our result agrees rather well with mean-field predictions [27,28]; see Fig. 4. More importantly, we can compare with the finite-β Hybrid Monte Carlo simulations at $\mu = 0$ (which are sign-problem free) performed on $N_t = 2$ and $N_t = 4$ [29–31] lattices with isotropic actions (i.e., $aT = 1/2$ and $1/4$) and extrapolated to zero quark mass. These data points are marked in black in Fig. 4. We have also computed $aT_c(\mu = 0)$ ourselves, using HMC on anisotropic lattices. As Fig. 4 left shows, our $\mathcal{O}(\beta)$ determination of $aT_c(\mu = 0)$ agrees perfectly with the linear approximation to the HMC determination. But the latter shows significant curvature. To better approximate the exact result, we perform an empirical, exponential extrapolation $aT_c(\mu = 0, \beta)/aT_c(\mu = 0, \beta = 0) \approx \exp(\beta(d/d\beta)aT_c|_{\beta=0})$. As seen in Fig. 4 right, it turns out that this approximation, which includes a resummation of higher-order β contributions, follows the exact HMC result up to $\beta \sim 5$ (or $a \sim 0.3$ fm), where the lattice theory is much closer to continuum physics. We have applied the same procedure to determine $aT_c(\beta)$ at nonzero chemical potential. $d(aT_c)/d\beta$ is clearly not as large as when $\mu = 0$. In fact, $d(aT_c)/d\beta$ becomes consistent with zero as μ approaches μ_T. The tricritical point and the first order line seem to only weakly depend on β. Thus, $T_c(\mu = 0)/\mu_c(T = 0)$ decreases at $\mathcal{O}(\beta)$ towards its continuum value.

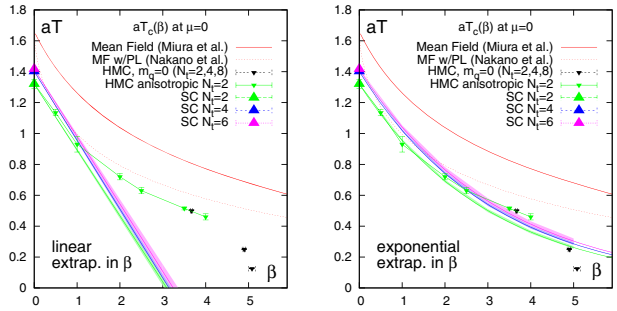

FIG. 4 (color online). Phase boundary in $\beta - aT$ plane at $\mu = 0$. Left: linear extrapolation. Right: exponential extrapolation. The boundary coincides very well with conventional Hybrid Monte Carlo data at large β. Also, the phase boundary is rather similar to the one obtained via a mean field theory approach without [27] and with Polyakov loop effects [28].

The resulting phase diagram is illustrated Fig. 5 for $\beta = 0.5$, 1.0, and 1.5. We show the phase boundary obtained by linear reweighting, based on Eq. (7), and that obtained by exponential extrapolation, which works so well at $\mu = 0$. In both cases, the phase boundary becomes more "rectangular" at weaker coupling: the second-order transition line becomes "flatter" (less μ dependent), and the first-order transition line remains almost "vertical," leaving the tricritical point at the "corner of the rectangle." From the chiral susceptibility, no clear shift of $(a\mu_T, aT_T) = (0.65(2), 0.91(5))$ could be detected; however, from the baryon density n_B [19], we have evidence that the critical

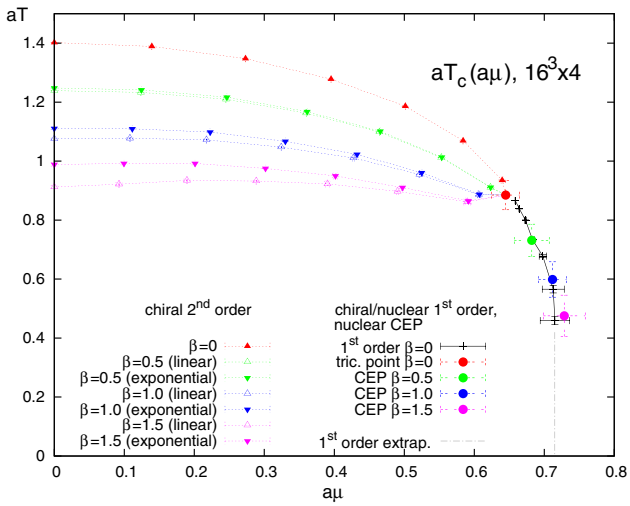

FIG. 5 (color online). Phase boundary in the $\mu - T$ plane in the strong coupling limit and extrapolated to finite β, comparing linear and exponential extrapolation. We do not observe a shift of the chiral tricritical point. The nuclear critical end point (CEP), determined from the reweighted baryon density, moves down along the first order line (extrapolated to $T = 0$ to guide the eye) as β is increased.

end point of the nuclear transition, which coincides with the chiral transition at $\beta = 0$, moves along the first order line, to smaller values of T. This is expected: as β increases, the lattice spacing a shrinks, and (aM_B) also, where M_B is the baryon mass. If $(a\mu_c)$ stays approximately constant as we observe, then the nuclear attraction responsible for the difference $[M_B - 3\mu_c(T = 0)]$, of about 300 MeV when $\beta = 0$ [7], becomes weaker. The weakening of the associated first-order transition brings the nuclear critical end point down in temperature.

We plan to study $\mathcal{O}(\beta^2)$ corrections next.

We would like to thank K. Miura and A. Ohnishi for helpful discussions. This work is supported by the Swiss National Science Foundation under Grant No. 200020-149723 and the Helmholtz International Center for FAIR within the LOEWE program launched by the State of Hesse.

[1] P. de Forcrand, *Proc. Sci.*, LATT2009 (2009) 010 [arXiv:1005.0539].
[2] M. Fromm, J. Langelage, S. Lottini, and O. Philipsen, J. High Energy Phys. 01 (2012) 042.
[3] M. Fromm, J. Langelage, S. Lottini, M. Neuman, and O. Philipsen, Phys. Rev. Lett. **110**, 122001 (2013).
[4] P. Rossi and U. Wolff, Nucl. Phys. **B248**, 105 (1984).
[5] U. Wolff, Phys. Lett. **153B**, 92 (1985).
[6] J. Langelage, M. Neuman, and O. Philipsen, arXiv:1403.4162.
[7] P. de Forcrand and M. Fromm, Phys. Rev. Lett. **104**, 112005 (2010).
[8] Y. Delgado Mercado, C. Gattringer, and A. Schmidt, Phys. Rev. Lett. **111**, 141601 (2013).
[9] K. E. Eriksson, N. Svartholm, and B. S. Skagerstam, J. Math. Phys. (N.Y.) **22**, 2276 (1981).
[10] F. Karsch and K. H. Mütter, Nucl. Phys. **B313**, 541 (1989).
[11] N. Kawamoto and J. Smit, Nucl. Phys. **B192**, 100 (1981).
[12] P. H. Damgaard, D. Hochberg, and N. Kawamoto, Phys. Lett. **158B**, 239 (1985).
[13] N. Bilic, F. Karsch, and K. Redlich, Phys. Rev. D **45**, 3228 (1992).
[14] N. Bilic, K. Demeterfi, and B. Petersson, Nucl. Phys. **B377**, 651 (1992).
[15] Y. Nishida, Phys. Rev. D **69**, 094501 (2004).
[16] A. Ohnishi, K. Miura, T. Nakano, and N. Kawamoto, *Proc. Sci.*, LATT2009 (2009) 160 [arXiv:0910.1896].
[17] D. H. Adams and S. Chandrasekharan, Nucl. Phys. **B662**, 220 (2003).
[18] W. Unger and P. de Forcrand, *Proc. Sci.*, LATT2011 (2011) 218 [arXiv:1111.1434].
[19] See Supplemental Material at http://link.aps.org/supplemental/10.1103/PhysRevLett.113.152002 for details on the anisotropy, the scaling analysis, and the baryon density.
[20] S. I. Azakov and E. S. Aliev, Phys. Scr. **38**, 769 (1988).
[21] M. Creutz, J. Math. Phys. (N.Y.) **19**, 2043 (1978).
[22] J. Langelage, Ph.D. thesis, Westfälische Wilhelms-Universität Münster, 2009.
[23] P. de Forcrand, S. Kim, and W. Unger, J. High Energy Phys. 02 (2013) 051.
[24] M. Fromm, J. Langelage, O. Philipsen, P. de Forcrand, W. Unger, and K. Miura, *Proc. Sci.*, LATT2011 (2011) 212 [arXiv:1111.4677].
[25] T. Hell, K. Kashiwa, and W. Weise, Phys. Rev. D **83**, 114008 (2011).
[26] C. Borgs and R. Kotecky, J. Stat. Phys. **61**, 79 (1990).
[27] K. Miura, T. Z. Nakano, A. Ohnishi, and N. Kawamoto, Phys. Rev. D **80**, 074034 (2009).
[28] T. Z. Nakano, K. Miura, and A. Ohnishi, Phys. Rev. D **83**, 016014 (2011).
[29] S. A. Gottlieb, W. Liu, D. Toussaint, R. L. Renken, and R. L. Sugar, Phys. Rev. D **35**, 3972 (1987).
[30] R. V. Gavai, S. Gupta, A. Irbäck, F. Karsch, S. Meyer, B. Petersson, H. Satz, and H. W. Wyld (MT(c) Collaboration), Phys. Lett. B **241**, 567 (1990).
[31] M. D'Elia and M.-P. Lombardo, Phys. Rev. D **67**, 014505 (2003).